The Linear Dynamics of Squall Line Mesohighs and Wake Lows

PATRICK T. HAERTEL AND RICHARD H. JOHNSON

Department of Atmospheric Science, Colorado State University, Fort Collins, Colorado

(Manuscript received 22 September 1998, in final form 16 April 1999)

ABSTRACT

Two surface pressure features that commonly accompany squall lines, the mesohigh and the wake low, may be explained at least in part as a linear response to the low-level cooling associated with stratiform precipitation. This response is numerically simulated for two- and three-dimensional, moving and stationary low-level coolings characteristic of squall line stratiform regions. When the cooling is defined to move and to have three-dimensional structure both a mesohigh and a mesolow develop, and their structures and evolutions resemble those of squall line mesohighs and wake lows. When an upper boundary is introduced directly above the cooling the response approaches a steady state in which a mesohigh–mesolow couplet is centered on the cooling. The simulations and the steady-state analysis presented here help to explain observed characteristics of squall line mesohighs and wake lows, including their life cycles and positioning relative to precipitation structures.

1. Introduction

a. Background

Much of the springtime rain over the central United States comes from systems that include a propagating line of vigorous convection, or squall line, and a trailing region of stratiform precipitation (Houze et al. 1990). Two intense surface pressure features referred to as the mesohigh and the wake low typically accompany such a system (Fujita 1955; Pedgley 1962; Williams 1963; Johnson and Hamilton 1988; Stumpf et al. 1991; Loehrer and Johnson 1995). Figure 1 depicts radar reflectivity, surface pressure, and surface winds within a mature squall system with the leading-line/trailing-stratiform organization. The mesohigh is centered just behind the convective line, and the wake low is centered on a strong gradient in reflectivity on the trailing edge of the stratiform region.

Mesohighs and wake lows evolve during a squall system's lifetime. Fujita (1955, 1963) identified five stages in a life cycle, four of which are depicted in Fig. 2. A weak mesohigh forms during the *initiation stage,* and it grows in scale and intensity during the *development stage.* Showers reach their maximum intensity during the *mature stage* and the wake low forms behind them. During the *dissipation stage* the precipitation and the mesohigh diminish, but the wake low reaches its maximum intensity. Finally, the wake low fills during the *remnant stage* (not shown). Pedgley (1962) observed a similar life cycle within squall systems over Great Britain, and Johnson and Hamilton (1988) also observed a squall system whose surface pressure features exhibited this life cycle.

The structure of surface pressure within a squall system is closely related to the pattern of precipitation. Loehrer and Johnson (1995) examined this relationship for 16 systems that passed over the central United States during May and June 1985. They constructed schemata for two radar-reflectivity patterns identified by Houze et al. (1990; Fig. 3). For the symmetric system the enhanced stratiform precipitation lies directly behind the convective line. For the asymmetric system the stratiform region is displaced to the left of the direction of propagation. For both systems the mesohigh–wake low couplet is approximately centered on the stratiform region.

Both mesohighs and wake lows are primarily hydrostatic in nature. Above the mesohigh the lower troposphere is cool and dense (Fujita 1959; Johnson and Hamilton 1988; Smull and Jorgensen 1990) and its excess weight per area accounts for most of the pressure surplus (Fujita 1959). This coolness has been attributed to the evaporation, melting, and sublimation of hydrometeors (Fujita 1959; Zhang and Gao 1989; Gallus 1996). While such phase changes of atmospheric water cool air locally, they also cause parcels to become negatively buoyant, to descend, and to transport the coolness downward (Rotunno et al. 1988). Gallus and Johnson (1991) measured the lower-tropopheric cooling (diabatic forcing) resulting from all of these processes both

Corresponding author address: Dr. Patrick Haertel, Department of Atmospheric Science, Colorado State University, Fort Collins, CO 80523-1371.
E-mail: haertel@thunder.atmos.colostate.edu

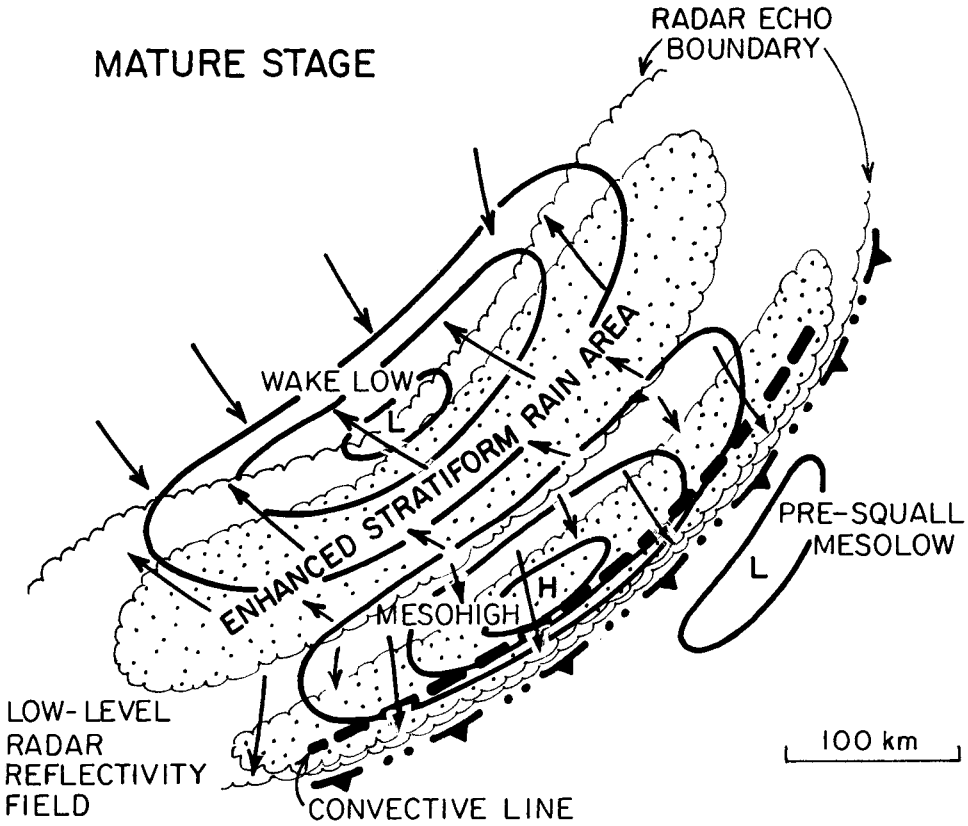

FIG. 1. Schema of a mature squall system (adapted from Johnson and Hamilton 1988). Surface pressure is contoured, vectors represent surface wind, and significant regions of precipitation are stippled.

in the convective line and the stratiform region of a squall system, and they found that while there was cooling in both places, the stratiform cooling was deeper and more intense. Other factors that can contribute to the mesohigh include the weight of hydrometeors (Sanders and Emanuel 1977) and nonhydrostatic pressure (Schaffer 1947).

The deficit in pressure within the wake low approximately equals the deficit in weight per area of a warm, not-so-dense lower troposphere (Williams 1963; Johnson and Hamilton 1988; Stumpf et al. 1991). There is a consensus that this lower-tropospheric warmth results from subsidence, but there are different ideas regarding the cause of the subsidence. Miller and Betts (1977) suggested that the subsidence is dynamically driven by the spreading of cold air near the surface. Johnson and Hamilton (1988) connected the subsidence to rear inflow into the system. Zhang and Gao (1989) called the wake low an ''end product of a chain of complicated dynamic reactions'' associated with latent cooling. Schmidt and Cotton (1990) attributed the subsidence and warming to gravity waves. Gallus (1996) showed that micro-

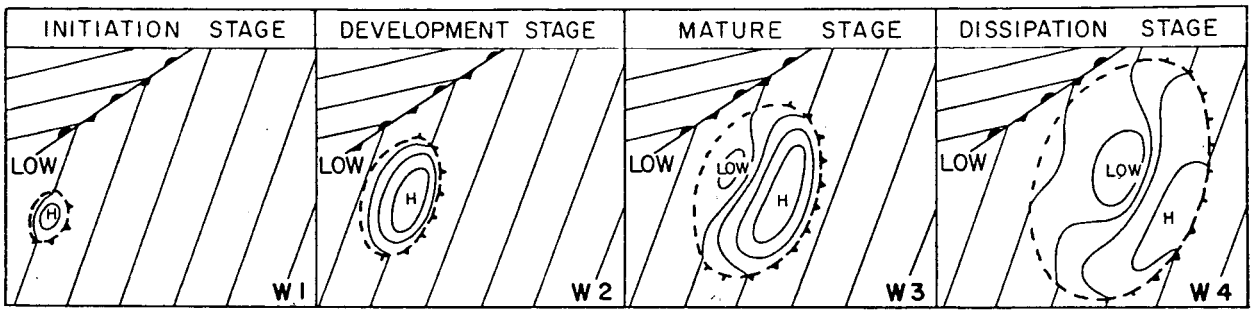

FIG. 2. Contours of surface pressure for four stages of a squall system (from Fujita 1963). The W denotes warm sector, i.e., the system formed on the warm side of a front.

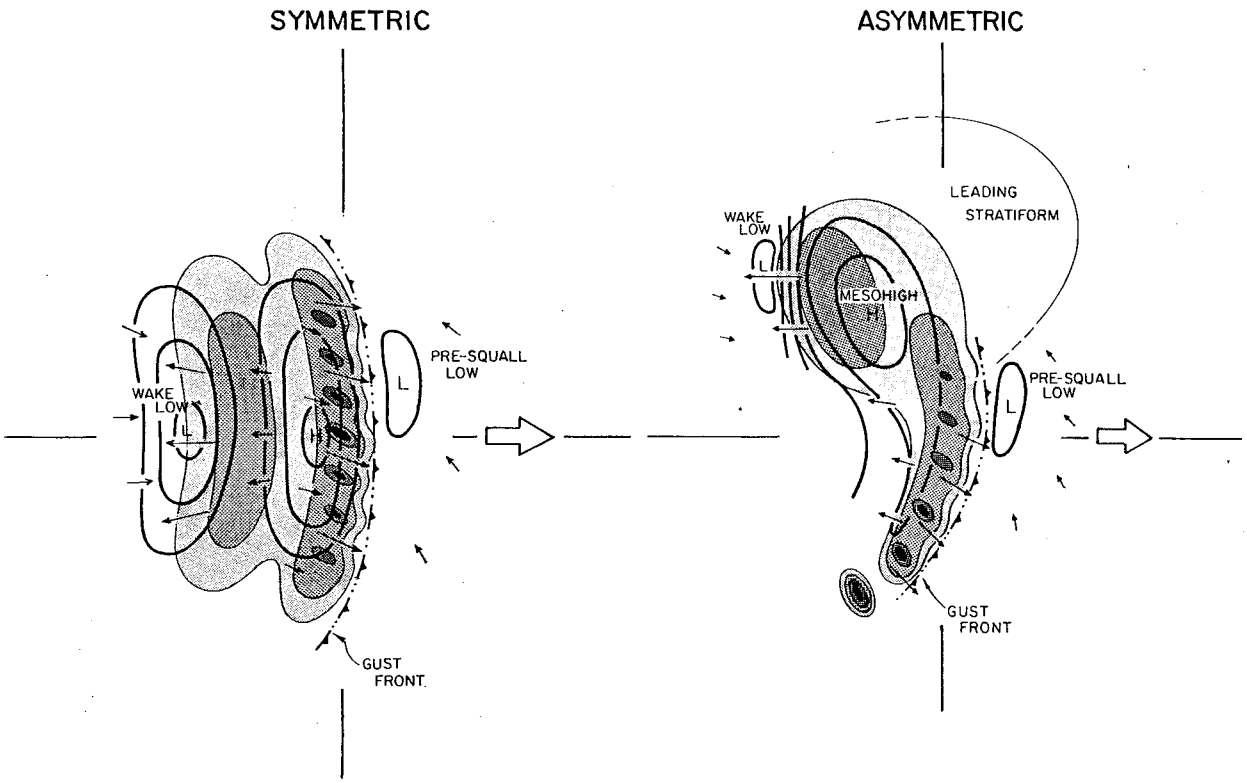

FIG. 3. Schemata of symmetric and asymmetric squall systems. Levels of shading denote increasing radar reflectivity, surface pressure is contoured with a 1-hPa interval, and vectors represent surface winds (from Loehrer and Johnson 1995).

physical processes within the stratiform region alone could generate strong subsidence, but only when the precipitation rates were prescribed to decrease with time did the subsidence generate significant lower-tropospheric warming.

b. Motivation

While previous studies have provided much information about squall line mesohighs and wake lows, their description of these surface pressure features is still lacking. They neither clarify the cause of the subsidence responsible for the wake low, nor do they explain the observed life cycles of mesohighs and wake lows (Fig. 2) or their positioning relative to precipitation structures (Fig. 3). In this paper we provide plausible explanations for each of these phenomena using linear dynamics. Using a simple numerical model we show that a portion of a squall system's thermal forcing, the low-level cooling associated with stratiform precipitation, can generate a linear response that includes a mesohigh–mesolow couplet similar to that observed in squall systems. We also present a steady-state analysis that predicts that such a couplet will develop in response to a moving, three-dimensional low-level cooling. Because of the ideal nature of the numerical simulations and the analysis presented here, one can fully understand their dynamics and in turn apply this understanding to squall line mesohighs and wake lows.

The numerical model is described in section 2, section 3 contains the simulations, the steady-state analysis is presented in section 4, and section 5 is a summary and discussion.

2. The numerical model

a. The equations

The numerical model is based on the hydrostatic Boussinesq equations linearized about a basic state of rest with a rigid upper boundary and no Coriolis force:

$$\frac{\partial D}{\partial t} + \frac{1}{\rho_0}\nabla^2 p = 0 \tag{1}$$

$$\frac{1}{\rho_0}\frac{\partial p}{\partial z} = b \tag{2}$$

$$\frac{\partial b}{\partial t} + wN^2 = Q \tag{3}$$

$$D + \frac{\partial w}{\partial z} = 0, \tag{4}$$

where ∇^2 is the horizontal Laplacian, D is horizontal

divergence, ρ_0 is the basic-state density (1.0 kg m^{-3}), p is perturbation pressure, b is buoyancy, w is vertical velocity, N is the buoyancy frequency (0.01 s^{-1}), and Q is the thermal forcing. At the lower and upper boundaries, w vanishes.

The linearization of (1)–(4) removed terms related to the vertical and horizontal advection of pertubation wind and buoyancy. For a consistency check we calculated the magnitude of these terms within the first simulation presented here and found them to be about half as intense as the related linear terms. Based on this calculation we conclude that while the linear approximation is consistent, we would expect nonlinear simulations to exhibit noticeable differences. Nevertheless, the linear dynamics studied here represent an important subset of the dynamics of more realistic nonlinear systems, and basing our simulations and analysis on (1)–(4) allows us to focus on this subset. Moreover, the simplicity of (1)–(4) allows for the analytical solution presented in section 4.

The system (1)–(4) is unrealistic in that the basic-state density ρ_0 is independent of height, whereas in the atmosphere density decreases exponentially with height. However, solutions to (1)–(4) may be converted to solutions to a version of the anelastic equations with a more realistic basic-state density simply by multiplying D, w, b, and Q by a fixed function of height (Nicholls et al. 1991). Since we focus on the lower troposphere where this conversion changes amplitudes by 20% or less (for our choice of ρ_0), we elected to use the simpler Boussinesq system.

Because the real atmosphere is unbounded, for most of the simulations we position the upper boundary sufficiently high (between 20 and 30 km) that the effects of the cooling barely reach it. However, solutions to (1)–(4) and their dynamical interpretation are greatly simplified when the upper boundary is placed directly above the cooling (at 4 km), and for the analytical interpretation in section 4 we place the boundary there.

We solve (1)–(4) using leapfrog time differencing (Δt = 60 s) and second-order spatial differencing (Δx = Δy = 10 km and Δz = 200 m). We arrived at the values for the time step and the grid spacing by reducing them until the numerical noise became negligible. In order to enforce the upper-boundary condition we require the vertical integral of p to be zero. The horizontal boundaries are periodic, but they are placed far enough away from the forcing to have little impact on the simulations.

b. The thermal forcing

Observations and simulations of the convectively generated thermal forcing within squall systems have revealed deep tropospheric heating above shallow cooling in the convective line, and upper-tropospheric heating and lower-tropospheric cooling in the stratiform region (Houze 1982; Gallus and Johnson 1991; Zhang et al. 1994; Pandya and Durran 1996). While the question of how the atmosphere responds to each and all of these components of thermal forcing is an interesting one, for this paper we have decided to focus on the response to the lower-tropospheric cooling associated with stratiform precipitation. Haertel and Johnson (1998) showed that the stratiform cooling has a much greater impact on surface pressure than either the convective or stratiform heating, and the results presented here establish that the response to the stratiform cooling can account for much of the surface pressure structure in the squall systems. We do not, however, assess the contribution of the convective cooling, which might also significantly alter surface pressure. Unlike the stratiform cooling it generally occurs in a neutral environment that is conducive to the formation of a gravity current (Raymond and Rotunno 1989), a nonlinear phenomenon that requires a more complicated dynamical system for simulation.

Although the movement and the horizontal structure of the coolings vary within the simulations presented here, for each case the cooling has a depth of 4 km, a vertical structure that resembles half of a sine wave, a horizontal scale of 150 km, and an amplitude of 3×10^{-5} m s^{-3}, which corresponds to about 3 K h^{-1} for a typical thermodynamic profile. Each of these aspects of the cooling is consistent with the budget calculations of Gallus and Johnson (1991). Numerical simulations (e.g., Zhang et al. 1994) have revealed the stratiform cooling to be more localized and intense, but considering that smoothing a squall system's thermal forcing in the horizontal seems to have little effect on the mesoscale structure of the atmospheric response (Pandya and Durran 1996), and that a broader, less intense thermal forcing is more consistent with the linear approximation, we elected to use a thermal forcing based on the budget calculations.

3. Simulations of the linear response to low-level cooling

This section contains four simulations; each is of the linear response to a low-level cooling characteristic of a stratiform region of a squall system. The dimensionality and movement of the coolings differ from one simulation to the next, and we emphasize that in order to generate a linear response that includes classic squall line mesohighs and wake lows the cooling must move and be three-dimensional.

a. Stationary, two-dimensional cooling

For the first simulation we define the thermal forcing as follows:

$$Q = Q_0 \exp(-\alpha^2 x^2) \sin(mz)$$

for $t \leq 4$ h and $z \leq 4$ km (the forcing is zero elsewhere and at later times), where $Q_0 = -3 \times 10^{-5}$ m s^{-3}, α = (75 km)$^{-1}$, and $m = \pi$ (4 km)$^{-1}$. This forcing rep-

resents the low-level cooling associated with a stationary, two-dimensional stratiform region with a width of 150 km. Its duration, which is shorter than that of a typical squall line stratiform region (6–8 h), was selected because it is sufficiently long to illustrate the dynamics of the response to the cooling and short enough that the response does not spread across the periodic boundaries of the model.

After 2 h, the response includes a negative buoyancy anomaly in the vicinity of the cooling (Fig. 4a), high surface pressure below this anomaly (Fig. 4b), and a region of low-level subsidence above the surface high that is bordered by weak upward motion on either side (Fig. 4c). There is also a small positive buoyancy anomaly above the cooling that is attributable to subsidence (Fig. 4a). After 4 h, the low-level bouyancy anomaly and the accompanying surface high have grown to be about 600 km across (Figs. 4d,e). By this time the subsidence has intensified and covers a larger area, while the regions of upward motion have moved farther away from the center of the cooling (Fig. 4f). While the negative buoyancy in the vicinity of the cooling can be attributed to direct thermal forcing, the remote reduction in buoyancy to either side of the cooling is a consequence of upward motion.

By 6 h (2 h after the cooling has ended) the low-level buoyancy anomaly has divided in two (Fig. 4g) and the resulting anomalies have propagated away from the location of the cooling. Each anomaly is accompanied by high surface pressure and has upward motion on its leading edge and subsidence on its trailing edge (Figs. 4h,i). The buoyancy anomalies and their accompanying pressure and vertical-motion structures are gravity waves, and their phase speed equals 13 m s^{-1} or N/m where m is their vertical wavenumber. Nicholls et al. (1991) previously noted that a stationary two-dimensional thermal forcing with finite duration generates two gravity waves that propagate away from the location of the forcing. The anomalies in buoyancy, pressure, and vertical motion that radiate up and away from where the cooling had been (Figs. 4g–i) represent the vertical propagation of gravity wave energy.

b. Moving, two-dimensional cooling

In this section we examine how the response to the two-dimensional cooling changes when the cooling moves. We define the thermal forcing as follows:

$$Q = Q_0 \exp[-\alpha^2(x - ct)^2] \sin(mz)$$

for $t \leq 4$ h and $z \leq 4$ km (the forcing is zero elsewhere and at later times), where Q_0, α, and m are as before, and $c = 10$ m s^{-1}.

After 2 h, the simulated fields of buoyancy, pressure, and vertical motion (Figs. 5a–c) resemble those in the previous simulation, although all fields are no longer symmetric about a central point; they are more intense in the direction of the cooling's movement. By 4 h the asymmetries have grown and the low-level buoyancy anomaly has an intense local minimum at $x = 150$ km, $z = 2$ km (Fig. 5d). Beneath this local minimum in buoyancy surface pressure exceeds 3 hPa (Fig. 5e), and trailing the buoyancy minimum low-level subsidence exceeds 27 cm s^{-1} (Fig. 5f). When the cooling shuts off at 4 h, just as before, the low-level buoyancy anomaly divides in two (Fig. 5g) as two gravity waves propagate away from the location of the cooling. While the cooling was generating the right-moving wave, it moved along with this wave, and this wave has become more intense than the left-moving wave (Figs. 5g–i). This simulation has illustrated how a moving forcing can generate a more intense response than a stationary forcing of the same magnitude.

An apparent gravity wave similar to the right-moving wave depicted in Figs. 5d–f) was observed within a squall system over the central United States on 3–4 June 1985 (Smull and Jorgensen 1990). Within that system the stratiform precipitation was accompanied by an intense negatative low-level buoyancy anomaly that was about 4 km deep. Just as in the simulation there was high pressure beneath the anomaly and strong subsidence on its trailing edge.

c. Stationary, axisymmetric cooling

Until now we have considered only two-dimensional coolings. In this section we define the cooling to be three-dimensional:

$$Q = Q_0 \exp(-\alpha^2x^2 - \alpha^2y^2) \sin(mz)$$

for $t \leq 4$ h and $z \leq 4$ km (the forcing is zero elsewhere and at later times), where Q_0, α, and m are as before. This forcing represents the lower-tropospheric cooling associated with a stationary, axisymmetric stratiform region with a diameter of 150 km.

Qualitatively, the response at 2 h (Figs. 6a–c) is quite similar to the response to the stationary, two-dimensional cooling at 2 h (Figs. 4a–c). For both cases there is negative bouyancy in the vicinity of the forcing that is accompanied by low-level subsidence and high surface pressure. There are, however, significant quantitative differences. For the axisymmetric case the low-level buoyancy anomaly (Fig. 6a) and the accompanying surface high (Fig. 6b) are weaker, owing to stronger low-level subsidence (Fig. 6c). The subsidence is stronger for this case because the cooling has generated a low-level pressure field with a negative second derivative in both the x and the y directions, which has generated greater low-level divergence according to (1), and therefore greater subsidence according to (4). At 4 h the quantitative differences between the two simulations are even greater. For the axisymmetric case the low-level buoyancy anomaly (Fig. 6d) and the accompanying surface high (Fig. 6e) are weaker than they were at 2 h, even though the cooling was maintained between these

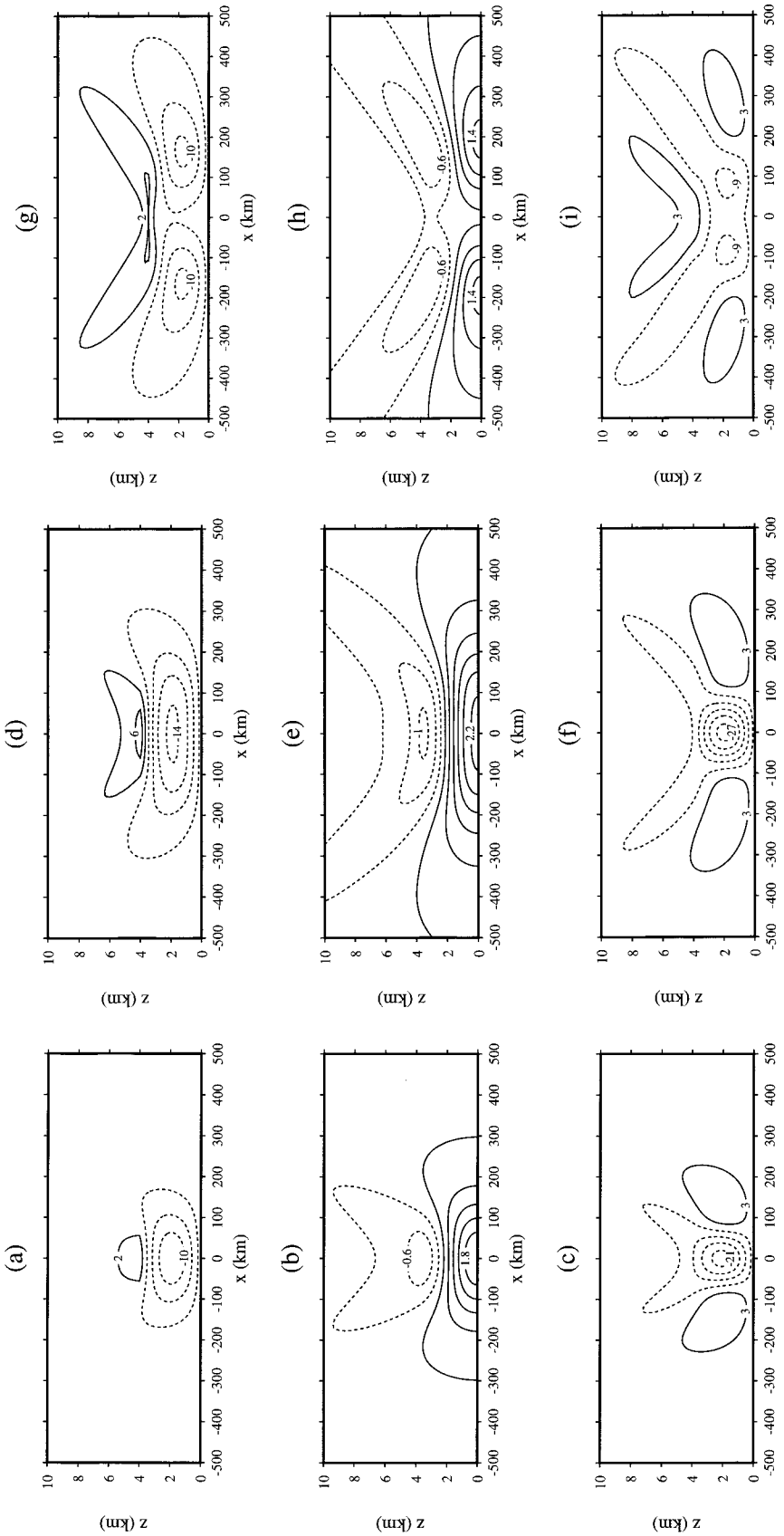

FIG. 4. The atmospheric response to the stationary, two-dimensional cooling: (a) buoyancy at 2 h with a 4 cm s^{-2} contour interval; (b) perturbation pressure at 2 h with a 0.4-hPa contour interval; (c) vertical velocity at 2 h with a 6 cm s^{-1} contour interval; (d) buoyancy at 4 h with a 4 cm s^{-2} contour interval; (e) perturbation pressure at 4 h with a 0.4-hPa contour interval; (f) vertical velocity at 4 h with a 6 cm s^{-1} contour interval; (g) buoyancy at 6 h with a 4 cm s^{-2} contour interval; (h) perturbation pressure at 6 h with a 0.4-hPa contour interval; and (i) vertical velocity at 6 h with a 6 cm s^{-1} contour interval.

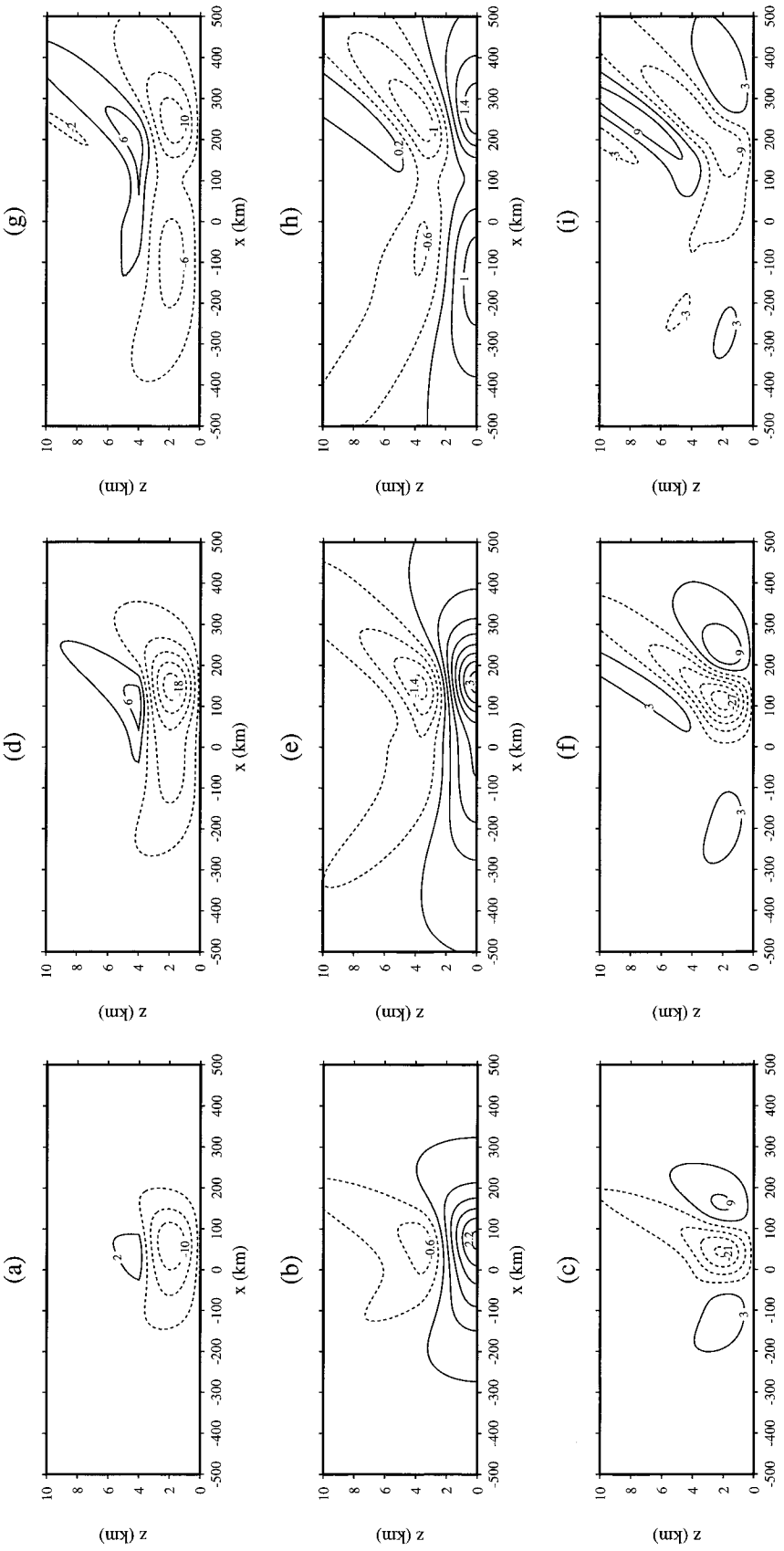

FIG. 5. The atmospheric response to the moving, two-dimensional cooling: (a) buoyancy at 2 h with a 4 cm s^{-2} contour interval; (b) perturbation pressure at 2 h with a 0.4-hPa contour interval; (c) vertical velocity at 2 h with a 6 cm s^{-1} contour interval; (d) buoyancy at 4 h with a 4 cm s^{-2} contour interval; (e) perturbation pressure at 4 h with a 0.4-hPa contour interval; (f) vertical velocity at 4 h with a 6 cm s^{-1} contour interval; (g) buoyancy at 6 h with a 4 cm s^{-2} contour interval; (h) perturbation pressure at 6 h with a 0.4-hPa contour interval; and (i) vertical velocity at 6 h with a 6 cm s^{-1} contour interval.

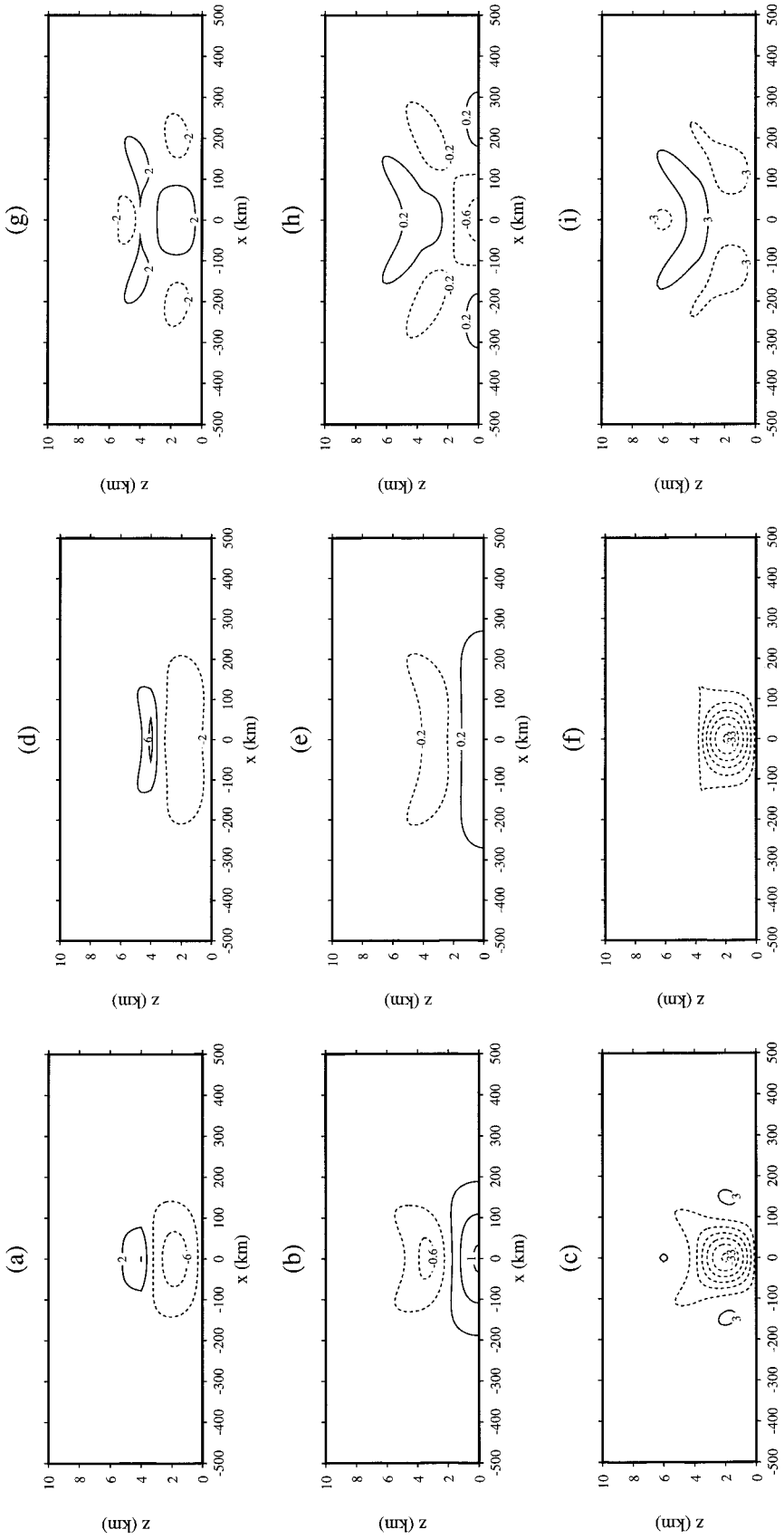

FIG. 6. The atmospheric response to the stationary, axisymmetric cooling along $y = 0$: (a) buoyancy at 2 h with a 4 cm s^{-2} contour interval; (b) perturbation pressure at 2 h with a 0.4-hPa contour interval; (c) vertical velocity at 2 h with a 6 cm s^{-1} contour interval; (d) buoyancy at 4 h with a 4 cm s^{-2} contour interval; (e) perturbation pressure at 4 h with a 0.4-hPa contour interval; (f) vertical velocity at 4 h with a 6 cm s^{-1} contour interval; (g) buoyancy at 6 h with a 4 cm s^{-2} contour interval; (h) perturbation pressure at 6 h with a 0.4-hPa contour interval; and (i) vertical velocity at 6 h with a 6 cm s^{-1} contour interval.

two times. The warming associated with the subsidence (Fig. 6f) has more than compensated for the cooling.

At 6 h the response to the stationary, axisymmetric cooling (Figs. 6g–i) is qualitatively different from the response to the stationary, two-dimensional cooling (Figs. 6g–i). In the axisymmetric case there is positive buoyancy (Fig. 6g) and negative surface pressure (Fig. 6h) where the cooling (diabatic forcing) had been, whereas in the two-dimensional case the buoyancy field remains negative (Fig. 4g), and the surface pressure field remains positive there (Fig. 4h). Once again these differences can be attributed to the greater subsidence of the axisymmetric case. This simulation has illustrated how an axisymmetric low-level cooling can generate low-level warmth (positive buoyancy) once the cooling has been shut off.

The fields of buoyancy and surface pressure within this simulation resemble those observed within a squall system over the central United States on 23–24 June 1985 (Johnson et al. 1989). At about 0500 UTC on 24 June a region of stratiform precipitation developed over southwestern Kansas and northwestern Oklahoma. It lasted for several hours, moving little, and then rapidly dissipated. A mesohigh developed beneath the stratiform region, and after the precipitation ended a mesolow formed where the mesohigh had been. Soundings taken in the vicinity of the mesohigh and mesolow showed that this pressure fall was a consequence of lower-tropospheric warming.

d. Moving, axisymmetric cooling

The preceding simulations have illustrated how a moving cooling can generate a more intense response than a stationary cooling of the same magnitude, and how a three-dimensional cooling can generate low-level warmth and negative perturbation surface pressure. In this section we show that when the cooling is defined to both move and to be three-dimensional, as is typical of the low-level coolings associated with squall line stratiform regions, the surface pressure response includes both a mesohigh and a mesolow that resemble squall line mesohighs and wake lows in structure and evolution.

We define the thermal forcing as follows:

$$Q = Q_0 \exp[-\alpha^2(x - ct)^2 - \alpha^2 y^2] \sin(mz)$$

for $t \leq 4$ h and $z \leq 4$ km (the forcing is zero elsewhere and at later times), where Q_0, α, and m are as before, and $c = 10$ m s^{-1}. As before, defining the forcing to move introduces asymmetry to the response, and at 2 h anomalies in buoyancy, pressure, and vertical motion resemble those for the stationary case but are more intense toward the direction of motion (Figs. 7a–c). By 4 h, unlike the stationary case, perturbations in all fields are largely confined to the vicinity of the cooling, which is centered at 144 km (Figs. 7d–f). In addition, the low-level buoyancy anomaly and the accompanying surface high are much more intense. After the cooling ends, a low-level positive buoyancy anomaly develops near $x = 100$ km (Fig. 7g), which has negative perturbation surface pressure below it (Fig. 7h). The low-level subsidence has become much weaker by this time (Fig. 7i).

The surface pressure response to the moving, axisymmetric forcing is shown in Fig. 8. At 2 h surface pressure exceeds 1.1 hPa within a mesohigh that is beneath the cooling, which is centered at $x = 76$ km, $y = 0$ km, at this time (Fig. 8a). By 4 h a local minimum in surface pressure has developed on the left edge of the forcing, which is now located at $x = 152$ km, $y = 0$ km (Fig. 8b). The mesohigh has intensified and shifted eastward, so that the maximum in surface pressure is located ahead of the center of the cooling. After the cooling shuts off at 4 h, as in the previous simulation, surface pressure falls rapidly in its vicinity, reaching a minimum of less than -0.8 hPa (Fig. 8c).

The evolution of surface pressure within this simulation is quite similar to that observed within squall systems (Fig. 2), with the mesohigh forming first and the mesolow becoming most intense after the forcing has dissipated. The pressure dipole at 4 h (Fig. 8b) also resembles those shown in Fig. 3, which are centered on regions of stratiform precipitation. By regarding this simulation as one of the surface pressure field in a squall system, we can use it to provide possible explanations for the life cycles of mesohighs and wake lows, their positioning relative to the stratiform region, and the subsidence that forms the wake low. By (2) pressure perturbations are the consequence of buoyancy perturbations, and by (3) buoyancy changes in one of two ways: by direct forcing or by vertical motion. Early in the simulation, vertical motion is weak, and a low-level negative buoyancy anomaly and accompanying mesohigh develop as a consequence of direct thermal forcing. If the vertical motion were to remain weak a swath of low-level coolness (negative buoyancy) and high surface pressure would trail the cooling. This, of course, is not what happens. Low-level upward motion develops ahead of the forcing, which decreases low-level buoyancy and increases surface pressure there. Subsidence develops in the vicinity of the forcing, and after the forcing shuts off, the subsidence more than erases the low-level negative buoyancy anomaly that the upward motion and direct forcing had generated. *So at least in this simulation, the structure of the mature mesohigh–mesolow couplet is determined more by vertical motion than by direct thermal forcing.* So what causes the subsidence responsible for the wake low? By (4) low-level subsidence is coincident with low-level divergence, and by (1) low-level divergence develops where the Laplacian of pressure is negative. This condition holds near local maxima in pressure and thus near the mesohigh. *So the low-level divergence and subsidence develop in response to the mesohigh, and because the horizontal flow has inertia (there is no vertical inertia in this sys-*

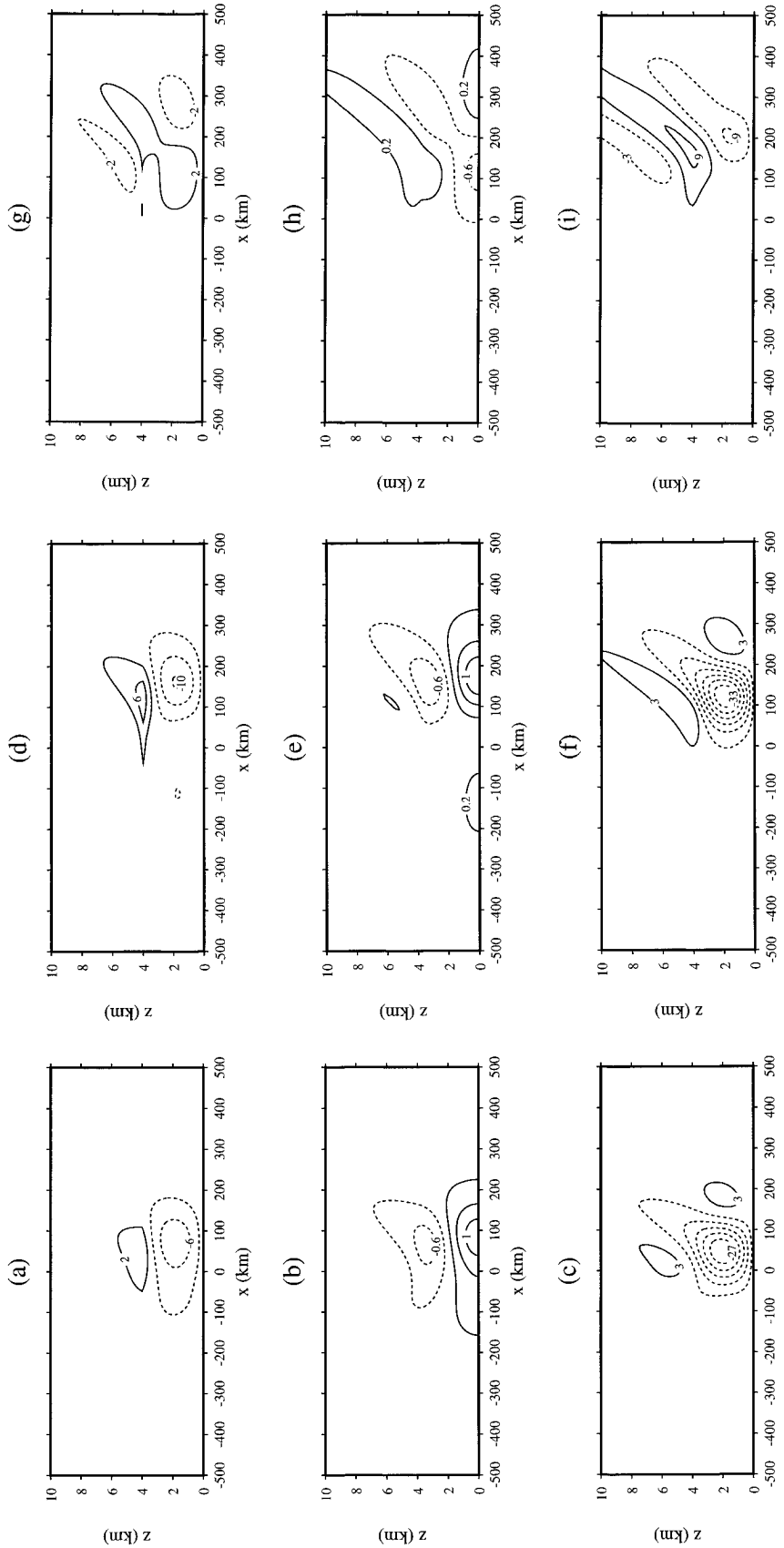

FIG. 7. The atmospheric response to the moving, axisymmetric cooling along $y = 0$: (a) buoyancy at 2 h with a 4 cm s^{-2} contour interval; (b) pressure at 2 h with a 0.4-hPa contour interval; (c) vertical velocity at 2 h with a 6 cm s^{-1} contour interval, where positive contours are solid and negative contours are dashed; (d) buoyancy at 4 h with a 4 cm s^{-2} contour interval; (e) pressure at 4 h with a 0.4-hPa contour interval; (f) vertical velocity at 4 h with a 6 cm s^{-1} contour interval; (g) buoyancy at 6 h with a 4 cm s^{-2} contour interval; (h) pressure at 6 h with a 0.4-hPa contour interval; and (i) vertical velocity at 6 h with a 6 cm s^{-1} contour interval.

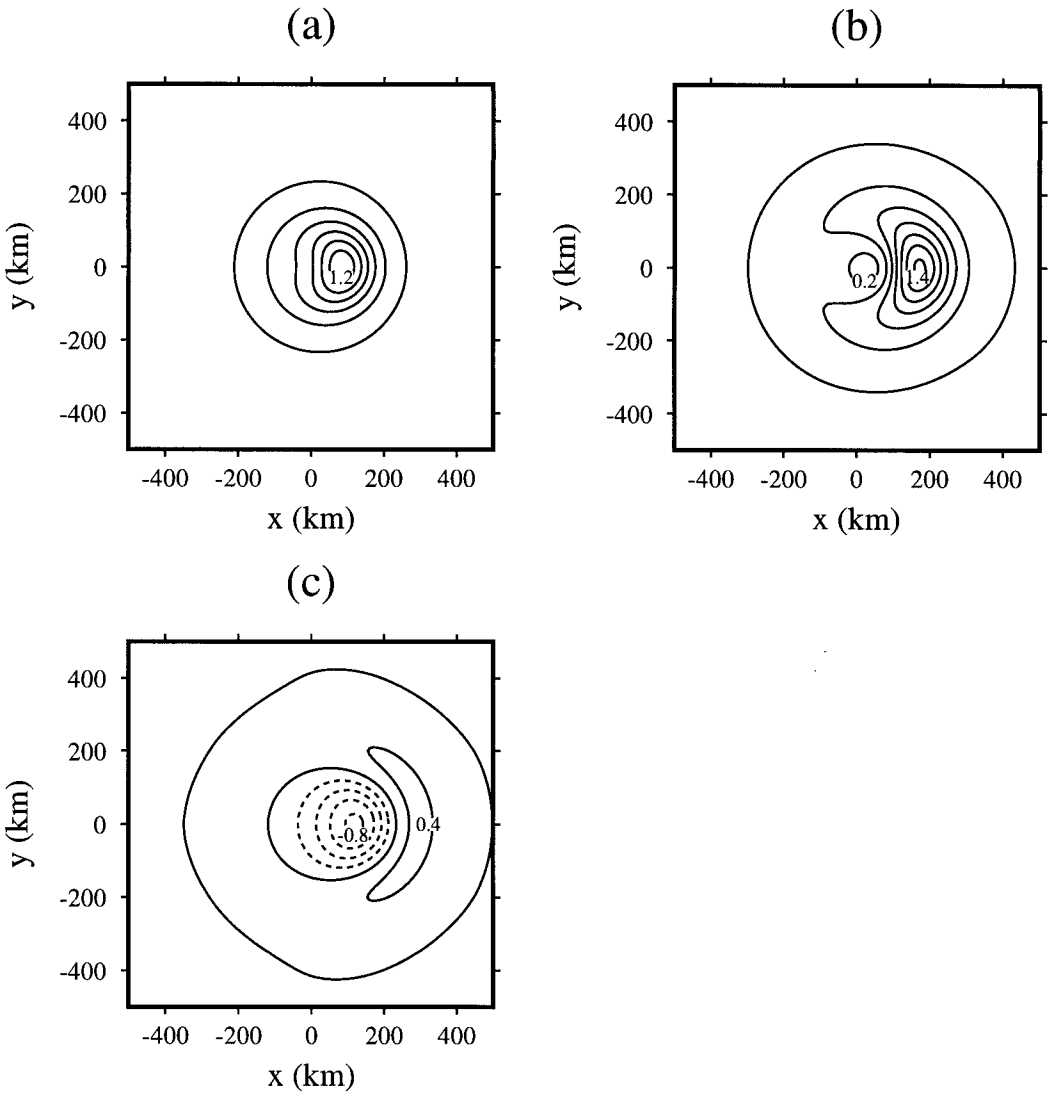

FIG. 8. The surface pressure response to the moving, axisymmetric cooling at (a) 2, (b) 4, and (c) 6 h. The contour interval is 0.2 hPa.

tem) they continue for a while after the mesohigh has dissipated.

4. An analytical interpretation of the mesohigh–wake low couplet

In the previous section we saw how a moving, axisymmetric low-level cooling generates a surface pressure response similar to that observed within squall systems. After several hours this response includes a dipole in surface pressure near the cooling. In this section we seek to understand this dipole and, accordingly, to understand the mesohigh–wake low couplet analytically. We begin by repeating the final simulation of the last section with two changes that facilitate simpler analytical interpretation: 1) the upper boundary is moved to 4 km (just above the cooling) and 2) the cooling never shuts off. Since repositioning the upper boundary does not significantly alter the low-level response for a number of hours, we contend that the simulation is still applicable to squall line mesohighs and wake lows.

Qualitiatively, the fields of buoyancy, pressure, and vertical motion remain unchanged below 4 km before 4 h (not shown). As before, the surface pressure response includes a mesohigh that is centered beneath the cooling at 2 h (Fig. 9a) and that moves ahead of the cooling by 4 h (Fig. 9b), in addition to a mesolow that develops on the left edge of the cooling just before 4 h (Fig. 9b). Because gravity wave energy can no longer radiate upward from the cooling (which leads to a horizontal smoothing of all fields), the surface pressure features are more intense than they were in the previous simulation.

After 4 h the mesohigh–mesolow couplet appears to

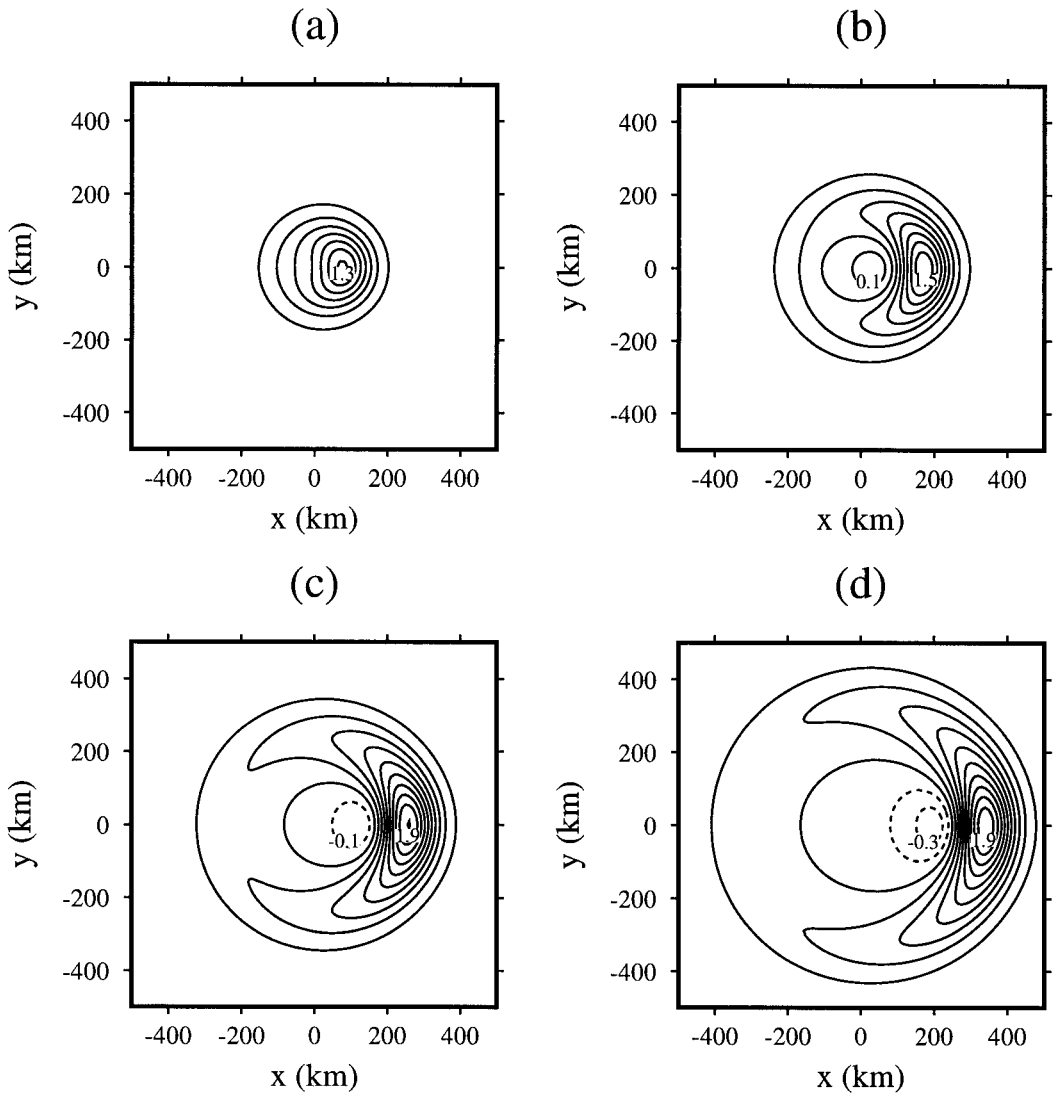

FIG. 9. The surface pressure response to the moving, axisymmetric cooling with the upper boundary directly above it at (a) 2, (b) 4, (c) 6, and (d) 8 h. The contour interval is 0.2 hPa.

be approaching a steady state within the frame of reference of the cooling (Figs. 9c,d). To solve for the steady-state response we transform Eqs. (1)–(4) into that frame of reference ($x' = x - ct$, $y' = y$, $z' = z$, $t' = t$):

$$\left(\frac{\partial}{\partial t'} - c\frac{\partial}{\partial x'}\right)D + \frac{1}{\rho_0}\nabla^2 p = 0 \tag{5}$$

$$\frac{1}{\rho_0}\frac{\partial p}{\partial z'} = b \tag{6}$$

$$\left(\frac{\partial}{\partial t'} - c\frac{\partial}{\partial x'}\right)b + wN^2 = Q \tag{7}$$

$$D + \frac{\partial w}{\partial z'} = 0. \tag{8}$$

For the remainder of this section we use only the moving coordinate system, and for convenience we neglect the prime notation. Combining (6)–(8) yields

$$\left(\frac{\partial}{\partial t} - c\frac{\partial}{\partial x}\right)\frac{1}{\rho_0}\frac{\partial^2 p}{\partial z^2} - DN^2 = \frac{\partial Q}{\partial z}. \tag{9}$$

For a given thermal forcing, (5) and (9) form a closed system. Next we assume that p and D have the following forms:

$$p(x, y, z, t) = \hat{p}(x, y, t)\cos(mz) \tag{10}$$

$$D(x, y, z, t) = \hat{D}(x, y, t)\cos(mz), \tag{11}$$

where $\hat{p}$ is surface pressure, $\hat{D}$ is surface divergence, and m is as before. Substituting into (5) and (9) using (10) and (11) yields

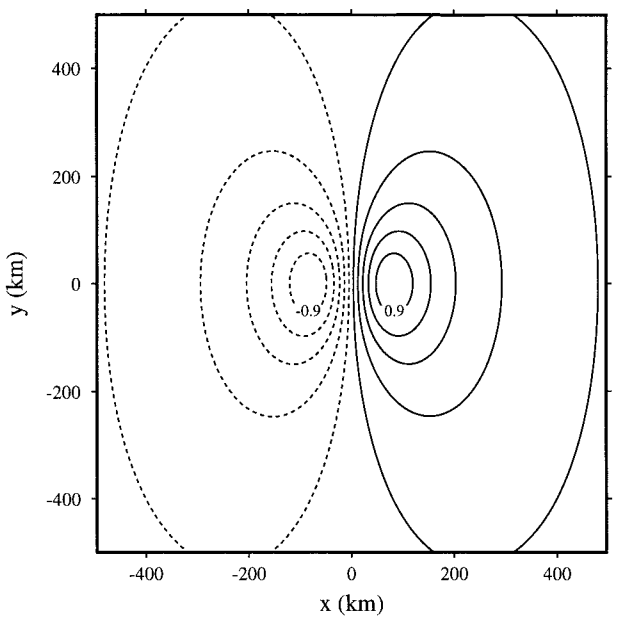

FIG. 10. The steady-state surface pressure response to the moving, axisymmetric cooling with the upper boundary directly above it. The contour interval is 0.2 hPa.

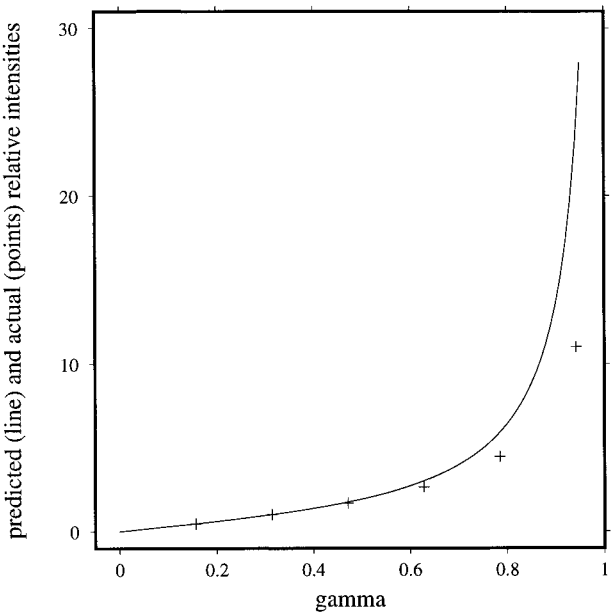

FIG. 11. A comparision of the relative intensities of the steady-state surface pressure responses to axisymmetric coolings to a theoretical curve based on the idea that the intensity is proportional to $\gamma/(1-\gamma^2)$. Each set of intensities is normalized about the point with $\gamma = 0.31$ ($c = 4$ m s^{-1}).

$$\left(\frac{\partial}{\partial t} - c\frac{\partial}{\partial x}\right)\hat{D} + \frac{1}{\rho_0}\nabla^2\hat{p} = 0 \tag{12}$$

$$\left(\frac{\partial}{\partial t} - c\frac{\partial}{\partial x}\right)\frac{1}{\rho_0}\hat{p} + \frac{N^2}{m^2}\hat{D} = -\frac{\hat{Q}}{m}, \tag{13}$$

where $\hat{Q} = Q_0 \exp(-\alpha^2x^2 - \alpha^2y^2)$. Equations (12) and (13) are algebraically equivalent to the irrotational shallow water equations. We are able to reduce (5)–(8) to this system because the vertical structure of the cooling is sinusoidal. Since we are interested in the steady-state solution we set the time derivatives to zero and solve for $\hat{p}$:

$$-\left\{\frac{\partial^2}{\partial x^2} + \frac{1}{1-\gamma^2}\frac{\partial^2}{\partial y^2}\right\}\hat{p} = \frac{\rho_0}{N}\frac{\gamma}{1-\gamma^2}\frac{\partial}{\partial x}\hat{Q}, \tag{14}$$

where $\gamma = cm/N$. We numerically solve (14) using Gauss-Seidel relaxation on a grid spaced so that $(\Delta x)^2 = (1-\gamma^2)(\Delta y)^2$.

The steady-state response includes a mesohigh ahead of the cooling and a mesolow trailing the cooling (Fig. 10; the cooling remains centered at the origin within the moving coordinate system). The transient solution begins to resemble the steady-state solution by 4 h (Fig. 9b) by which time a pressure dipole has appeared, and the resemblance increases with time as the mesolow intensifies (Figs. 9c,d). Since the response is approaching a steady state within the frame of reference of the cooling, both the mesohigh and the mesolow are becoming stationary within this frame of reference, which means they are moving at 10 m s^{-1} in the original coordinate system. This speed differs from the gravity wave speed associated with a half-vertical-wavelength of 4 km (13 m s^{-1}). Therefore, the steady state does not represent a single wave packet; rather it is reached when the rate at which the gravity waves disperse energy equals the rate at which the cooling adds energy.

Although we actually solved (14), we could have predicted the character of the steady-state response just by inspecting this equation. When $0 < \gamma < 1$ (for the simulation $\gamma = 0.785$) the terms inside the braces resemble a Laplacian, and we expect the right side of the equation to be roughly proportional to $\hat{p}$. Therefore, we expect $\hat{p}$ to be roughly proportional to the x derivative of the thermal forcing. The horizontal structure of the cooling is Gaussian, its x derivative is a dipole, and so is the steady-state surface-pressure response (Fig. 10).

By inspecting (14) one can also surmise how the intensity of the response depends on the speed of the forcing. The speed c determines γ, which appears on both sides of (14). The right side of (14) is proportional to $\gamma/(1-\gamma^2)$, so we might expect the intensity of the response to also be proportional to this factor. The parameter γ also appears on the left side of (14) where we would expect it to be a smoothing parameter and have a less direct impact on intensity. In order to test these ideas we solved (14) multiple times for the axisymmetric cooling, varying c so that γ varied between 0 and 1. Figure 11 shows the relative intensity of the response for each case along with a prediction of intensity made assuming it to be proportional to $\gamma/(1-\gamma^2)$. The prediction is very good for $0 < \gamma \leq 0.5$, fair

for $0.5 < \gamma < 0.8$, and poor for $\gamma > 0.8$. Even though the prediction overestimates intensity for $\gamma > 0.6$, it is clear that intensity increases rapidly as the speed of the cooling approaches the gravity speed associated with its vertical wavelength ($\gamma \rightarrow 1$); when $\gamma = 0.94$ the response to the axisymmetric cooling is 11 times as intense as it is when $\gamma = 0.31$.

Although the intensity of the steady-state response is quite sensitive to γ the structure of the response is not. For each value of c tested, the response included a mesohigh ahead of the cooling and a mesolow trailing the cooling. For every case each of these pressure features had the same positioning relative to the cooling and about the same scale (not shown); for every case the structure of surface pressure closely resembled that of the x derivative of the thermal forcing.

In this section we have seen that when the upper boundary is positioned just above the cooling, the response approaches a steady state within the frame of reference of the cooling. The structure of this response is not very sensitive to the speed of the cooling, but its intensity increases rapidly as the speed approaches the gravity wave speed associated with the cooling's vertical wavelength. So how does this result generalize to an ''unbounded'' atmosphere, that is, the limiting case in which the height of the upper boundary approaches infinity? When the upper boundary is not positioned just above the cooling, the cooling's vertical structure is no longer sinusoidal nor can it be represented as a finite sum of sinuisodal funcions, and the solution does not approach a steady state. However, gravity waves disperse energy horizontally in a similar manner so that the surface pressure response tends toward a dipole at least for a number of hours, and the response is in a quasi-steady state. Thus, one may regard the dipole in surface pressure that develops (Fig. 8b) as a quasi-steady-state response to the moving low-level cooling.

5. Summary and discussion

In this paper we have shown that squall line mesohighs and wake lows may be explained at least in part as a linear response to the low-level cooling associated with stratiform precipitation. We simulated this response for four low-level coolings characteristic of squall line stratiform regions. When the cooling was defined to move and to have three-dimensional structure, a mesohigh and a mesolow developed, and their structures and evolutions resembled those of squall line mesohighs and wake lows. The introduction of an upper boundary directly above the moving, three-dimensional cooling caused no qualitative change in the surface pressure response, and it allowed for an analytical, steady-state solution that included a mesohigh–mesolow couplet centered on the cooling.

Based on the simulations and the analysis presented here, we believe that a useful conceptual model of the squall line mesohigh–wake low couplet is as a quasi-steady-state linear response to low-level cooling associated with stratiform precipitation. This model is consistent with the schemata of symmetric and asymetric squall systems constructed by Loehrer and Johnson (1995; Fig. 3), each of which depicts a dipole in surface pressure centered on the stratiform region as the steady-state analysis predicts. This model also accounts for the life cycle observed by Fujita (1955, 1963), and it supports a dynamical explanation for the subsidence responsible for the wake low (as discussed in section 3d). The model is consistent with past studies of mesohighs and wake lows that emphasize the importance of low-level cooling in generating these pressure features (Zhang and Gao 1989; Gallus 1996) and how the horizontal inertia of low-level divergent flow drives the low-level subsidence in the wake of squall lines (Miller and Betts 1977).

While the linear theory presented here provides insight into the dynamics of mesohighs and wake lows, it does have significant limitations. Much of the dynamics of squall systems is nonlinear, and in particular, most are accompanied by a shallow layer of cold air near the surface (gravity current) whose advance is an advective, nonlinear process. For some systems (e.g., Fujita 1959) the mesohigh is largely attributable to such a gravity current and the applicability of linear theory is questionable. For others (e.g., Johnson and Hamilton 1988) the mesohigh seems to be the result of both shallow, intense coolness (a gravity current) and a deeper layer of coolness (a gravity wave), and the linear theory can explain a portion of the mesohigh. For still other systems, such as those studied by Pedgley (1962), gravity-current contributions to the mesohigh are probably small [Pedgley (1962) noted that surface temperature changes were ''quite small''], and the linear theory is most applicable.

Although gravity-current contributions to surface pressure perturbations may account for much of the mesohigh, they do not explain the wake low, which appears to be more aptly described as a gravity wave phenomenon. Moreover, even in systems accompanied by a strong gravity current, the linear theory may adequately describe the structure of surface pressure some distance back from the leading edge of the gravity current (e.g., the asymmetric system in Fig. 3). Thus, despite its limitations the linear theory of squall line mesohighs and wake lows presented here seems to explain at least a portion of their dynamics, and it is appealing because of its simplicity.

Acknowledgments. This research was supported by the National Oceanic and Atmospheric Administration under Grants NA67RJ0152 and NA37RJ0202, and by the National Science Foundation under Grant ATM-9618684. We thank Wayne Schubert, Dave Randall, Michael Montgomery, and two anonymous reviewers for their comments.

REFERENCES

Fujita, T. T., 1955: Results of detailed synoptic studies of squall lines. *Tellus,* **7,** 405–436.

——, 1959: Precipitation and cold air production in mesoscale thunderstorm systems. *J. Meteor.,* **16,** 454–466.

——, 1963: Analytical mesometeorology. A review. *Meteor. Monogr.,* No. 27, 77–125.

Gallus, W. A., Jr., 1996: The influence of microphysics in the formation of intense wake lows: A numerical modeling study. *Mon. Wea. Rev.,* **124,** 2267–2281.

——, and R. H. Johnson, 1991: Heat and moisture budgets of an intense midlatitude squall line. *J. Atmos. Sci.,* **48,** 122–146.

Haertel, P. T., and R. H. Johnson, 1998: The dynamics of surface pressure within squall systems. Preprints, *19th Conf. on Severe Local Storms,* Minneapolis, MN, Amer. Meteor. Soc., 392–394.

Houze, R. A., Jr., 1982: Cloud clusters and large-scale vertical motions in the tropics. *J. Meteor. Soc. Japan,* **60,** 396–410.

——, B. F. Smull, and P. Dodge, 1990: Mesoscale organization of springtime rainstorms in Oklahoma. *Mon. Wea. Rev.,* **118,** 613–654.

Johnson, R. H., and P. J. Hamilton, 1988: The relationship of surface pressure features to the precipitation and airflow structure of an intense midlatitude squall line. *Mon. Wea. Rev.,* **116,** 1444–1472.

——, S. Chen, and J. J. Toth, 1989: Circulations associated with a mature-to-decaying midlatitude mesoscale convective system. Part I: Surface features—Heat bursts and mesolow development. *Mon. Wea. Rev.,* **117,** 942–959.

Loehrer, S. M., and R. H. Johnson, 1995: Surface pressure and precipitation life cycle characteristics of PRE-STORM mesoscale convective systems. *Mon. Wea. Rev.,* **123,** 600–621.

Miller, M. J., and A. K. Betts, 1977: Traveling convective storms over Venezuela. *Mon. Wea. Rev.,* **105,** 833–848.

Nicholls, M. E., R. A. Pielke, and W. R. Cotton, 1991: Thermally forced gravity waves in an atmosphere at rest. *J. Atmos. Sci.,* **48,** 1869–1884.

Pandya, R., and D. Durran, 1996: The influence of convectively generated thermal forcing on the mesoscale circulations around squall lines. *J. Atmos. Sci.,* **53,** 2924–2951.

Pedgley, D. E., 1962: A meso-synoptic analysis of the thunderstorms on 28 August 1958. *British Meteorological Office Geophysical Memoirs,* **106,** 74 pp.

Raymond, D. J., and R. Rotunno, 1989: Response of a stably stratified flow to cooling. *J. Atmos. Sci.,* **46,** 2830–2837.

Rotunno, R., J. B. Klemp, and M. L. Weismann, 1988: A theory for strong, long-lived squall lines. *J. Atmos. Sci.,* **45,** 463–485.

Sanders, F., and K. A. Emanuel, 1977: The momentum budget and temporal evolution of a mesoscale convective system. *J. Atmos. Sci.,* **34,** 322–330.

Schaffer, W., 1947: The thunderstorm high. *Bull. Amer. Meteor. Soc.,* **28,** 351–355.

Schmidt, J. M. and W. R. Cotton, 1990: Interactions between upper and lower tropospheric gravity waves on squall line structure and maintenance. *J. Atmos. Sci.,* **47,** 1205–1222.

Smull, B. F., and D. P. Jorgensen, 1990: Pressure and buoyancy perturbations near an intense wake low in a midlatitude mesoscale convective system. *Extended Abstracts, Fourth Conf. on Mesoscale Processes,* Boulder, CO, Amer. Meteor. Soc., 214–215.

Stumpf, G. J., R. H. Johnson, and B. F. Smull, 1991: The wake low in a midlatitude convective system having complex convective organization. *Mon. Wea. Rev.,* **119,** 134–158.

Williams, D. T., 1963: The thunderstorm wake of May 4, 1961. National Severe Storms Project Rep. 18, U.S. Dept. of Commerce, Washington DC, 23 pp. [NTIS PB 168223.]

Zhang, D.-L., and K. Gao, 1989: Numerical simulation of an intense squall line during 10–11 June 1985 PRE-STORM. Part II: Rear inflow, surface pressure perturbations and stratiform precipitation. *Mon. Wea. Rev.,* **117,** 2067–2093.

——, J. S. Kain, J. M. Fritsch, and K. Gao, 1994: Comments on ''Parameterization of convective precipitation in mesoscale numerical models: A critical review.'' *Mon. Wea. Rev.,* **122,** 2222–2231.